The Astrophysical Journal, 981:48 (8pp), 2025 March 1 https://doi.org/10.3847/1538-4357/adaaef

The Radio Counterpart to the Fast X-Ray Transient EP240414a

Joe S. Bright[1,2], Francesco Carotenuto[1], Rob Fender[1,3], Carmen Choza[4], Andrew Mummery[5], Peter G. Jonker[6,7], Stephen J. Smartt[1,8], David R. DeBoer[9], Wael Farah[4,10], James Matthews[1], Alexander W. Pollak[4], Lauren Rhodes[1], and Andrew Siemion[1,2,4,10,11,12]

[1] Astrophysics, Department of Physics, The University of Oxford, Keble Road, Oxford OX1 3RH, UK; joe.bright@physics.ox.ac.uk
[2] Breakthrough Listen, Astrophysics, Department of Physics, The University of Oxford, Keble Road, Oxford OX1 3RH, UK
[3] Department of Astronomy, University of Cape Town, Private Bag X3, Rondebosch 7701, South Africa
[4] SETI Institute, 339 Bernardo Avenue, Suite 200, Mountain View, CA 94043, USA
[5] Oxford Theoretical Physics, Beecroft Building, Clarendon Laboratory, Parks Road, Oxford OX1 3PU, UK
[6] Department of Astrophysics/IMAPP, Radboud University, PO Box 9010, 6500 GL, Nijmegen, The Netherlands
[7] SRON, Netherlands Institute for Space Research, Niels Bohrweg 4, 2333 CA, Leiden, The Netherlands
[8] Astrophysics Research Centre, School of Mathematics and Physics, Queen's University Belfast, BT7 1NN, UK
[9] Radio Astronomy Lab, University of California, Berkeley, CA, USA
[10] Berkeley SETI Research Centre, University of California, Berkeley, CA 94720, USA
[11] Department of Physics and Astronomy, University of Manchester, UK
[12] University of Malta, Institute of Space Sciences and Astronomy, Msida, MSD2080, Malta
Received 2024 September 29; revised 2025 January 8; accepted 2025 January 14; published 2025 February 25

Abstract

Despite being operational for only a short time, the Einstein Probe mission, with its large field of view and rapid localization capabilities, has already significantly advanced the study of rapid variability in the soft X-ray sky. We report the discovery of luminous and variable radio emission from the Einstein Probe fast X-ray transient EP240414a, the second such source with a radio counterpart. The radio emission at 3 GHz peaks at ∼30 days postexplosion and with a spectral luminosity $\sim 2 \times 10^{30}$ erg s^{-1} Hz^{-1}, similar to what is seen from long gamma-ray bursts, and distinct from other extragalactic transients including supernovae and tidal disruption events, although we cannot completely rule out emission from engine driven stellar explosions, e.g., the fast blue optical transients. An equipartition analysis of our radio data reveals that an outflow with at least a moderate bulk Lorentz factor ($\Gamma \gtrsim 1.6$) with a minimum energy of $\sim 10^{48}$ erg is required to explain our observations. The apparent lack of a reported gamma-ray counterpart to EP240414a could suggest that an off-axis or choked jet could be responsible for the radio emission, although a low-luminosity gamma-ray burst may have gone undetected. Our observations are consistent with the hypothesis that a significant fraction of extragalactic fast X-ray transients are associated with the deaths of massive stars.

Unified Astronomy Thesaurus concepts: Extragalactic radio sources (508); Radio transient sources (2008); Relativistic jets (1390); X-ray transient sources (1852); Gamma-ray bursts (629); Transient sources (1851); High energy astrophysics (739)

1. Introduction

Fast X-ray transients (FXTs) are bursts of soft X-ray emission lasting tens to thousands of seconds and spanning a wide range of luminosities (J. Quirola-Vásquez et al. 2022, 2023). Typically discovered through searches of X-ray telescope data archives (particularly those of Chandra, XMM-Newton, Swift, and eROSITA), FXTs were only identified months or years after they occurred, and so prompt multi-wavelength follow-up has to date been sparse (although see A. M. Soderberg et al. 2008; D. Ibrahimzade et al. 2025). Based on the soft X-ray emission alone, a range of progenitor scenarios have been suggested for FXTs including white dwarf tidal disruption events (TDEs; P. G. Jonker et al. 2013; A. Glennie et al. 2015), stellar flares (A. Glennie et al. 2015), supernova shock breakout (A. M. Soderberg et al. 2008; D. Alp & J. Larsson 2020; G. Novara et al. 2020), long gamma-ray bursts (LGRBs; P. G. Jonker et al. 2013; F. E. Bauer et al. 2017), and newly born rapidly rotating magnetic neutron stars (Y. Q. Xue et al. 2019). The range of observed FXT luminosities (from 10^{30} erg s^{-1} for suspected stellar flares to 10^{48} erg s^{-1} for distant extragalactic events) likely supports a variety of progenitor systems, although this conclusion is made unclear by the difficulty in identifying a host galaxy for the majority of extragalactic FXTs to date (see, e.g., D. Eappachen et al. 2022, 2023, 2024; J. Quirola-Vásquez et al. 2023).

The observational paradigm for FXTs has recently undergone a drastic shift with the launch of the Einstein Probe (EP) X-ray telescope (W. Yuan et al. 2022). The two instruments on board the EP, the Wide Field X-ray Telescope (WXT) and the Follow-up X-ray Telescope (somewhat unfortunately abbreviated as FXT), allow for wide sky area monitoring as well as follow-up and localization regions that range from arcminutes to tens of arcseconds, with FXT candidates reported via public alert streams. These capabilities have allowed for rapid follow-up at optical, radio, and X-ray wavelengths and the detection of multiwavelength counterparts to EPW20240219aa, EP240305a, EP240309a, and EP240315a. The sources EP240305a and EP240309a are likely Galactic and have been associated with variability from a Gaia star (M. J. Liu et al. 2024) and a cataclysmic variable (D. A. H. Buckley et al. 2024), respectively. EPW20240219aa was associated with a subthreshold event by the Fermi Gamma-ray Burst Monitor and is therefore thought to

have been caused by a gamma-ray burst (GRB; C. Fletcher et al. 2024). EP240315a was associated with a high-redshift ($z \sim 4.9$) galaxy and was followed up across the electromagnetic spectrum, being the first EP FXT with a radio and optical counterpart (F. Carotenuto et al. 2024; J. H. Gillanders et al. 2024). Analysis of the radio, optical, and X-ray data led to the conclusion that the event harbored a relativistic jet and was likely from an LGRB (J. H. Gillanders et al. 2024; R. Ricci et al. 2025; A. J. Levan et al. 2024b; Y. Liu et al. 2025). With these events, and the increasing number of new events being discovered and quickly reported by the EP, it is clear that significant progress can now be made in understanding the progenitors to FXTs and their multiwavelength properties.

In this paper we present a radio observing campaign on EP240414a, the second EP extragalactic FXT with a multiwavelength counterpart. EP240414a was discovered (T. Y. Lian et al. 2024) by the WXT at UTC 09:50:12 2024 April 14 (MJD 60414.4099, which we define to be T_0) with a peak flux of $\sim 3 \times 10^{-9}$ erg s^{-1} cm^{-2} in the 0.5–4 keV energy band and was seen to fade by 4 dex over the following 2 hr with the EP Follow-up X-ray Telescope (J. Guan et al. 2024). An optical counterpart (AT2024gsa) was discovered within 3 hr of the FXT detection (A. Aryan et al. 2024), and a redshift of the nearest galaxy was reported to be $z = 0.41$ (P. G. Jonker et al. 2024). The rapid and unusual optical light curve of the source is reported in S. Srivastav et al. (2024) with the redshift confirmed to be $z = 0.4018 \pm 0.0010$ (see also J. N. D. van Dalen et al. 2024). This implies a peak X-ray luminosity of $\sim 10^{48}$ erg s^{-1}, similar to those seen from GRB afterglows at early times (see, e.g., N. Gehrels et al. 2009), at a projected offset of $\sim$27 kpc from the host (unusually large for an LGRB; J. S. Bloom et al. 2002; P. K. Blanchard et al. 2016; J. D. Lyman et al. 2017). We discovered the radio counterpart to EP240414a with the MeerKAT radio interferometer, 6 days after it was reported as an FXT by the EP, as a $\sim$200 μJy radio source coincident with the EP error circles (J. Guan et al. 2024; T. Y. Lian et al. 2024) and coincident with AT2024gsa (A. Aryan et al. 2024; J. Bright et al. 2024; S. Srivastav et al. 2024; J. N. D. van Dalen et al. 2024).

This paper describes our entire radio observing campaign on EP240414a. In Section 2 we present our radio observations from MeerKAT, the Australian Telescope Compact Array, and the Allen Telescope Array, as well as serendipitous observations from large sky area radio surveys. In Sections 3 and 4 we share our results and discuss the emission from EP240414a in the context of other extragalactic transients, and in Section 5 we present our conclusions. Throughout this work we assume a flat cosmology with $H_0 = 70$ km s^{-1} Mpc^{-1}, $T_{\rm CMB} = 2.725$ K, and $\Omega_{\rm m} = 0.3$. Distances are calculated using the `astropy.cosmology` package.

2. Observations

2.1. MeerKAT

The field of EP240414a was observed with the MeerKAT radio telescope under project ID SCI-20230907-JB-01 (PIs: Bright and Carotenuto), where we discovered the 3 GHz (using the S4 *S*-band receiver setup) radio counterpart to EP240414a on 2024 April 20 (J. Bright et al. 2024). The discovery radio image is shown in Figure 1, where we detect clear radio emission at the position of EP240414a (R.A. = 12:46:01.669, decl. = −09:43:08.88 from the Transient Name Server where the source is identified as

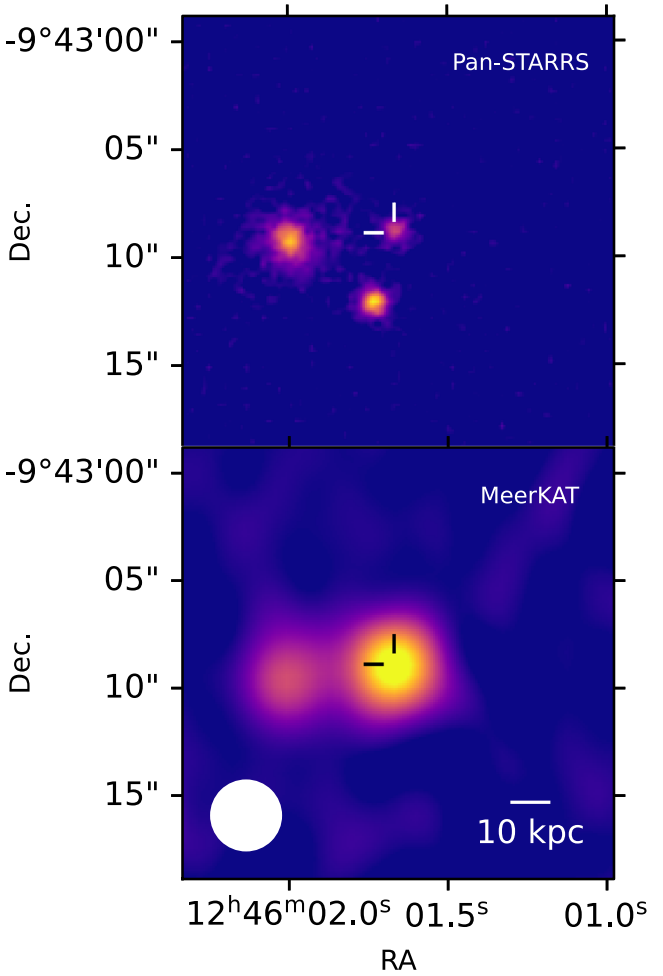

Figure 1. Optical and radio detections of EP240414a/AT2024gsa. (Top) A Pan-STARRS *i*-band image of the field of EP240414a. The source position is marked by a pair of white lines. The diffuse source to the left is the putative host galaxy Sloan Digital Sky Survey J124601.99−094309.3 (A. Aryan et al. 2024; P. G. Jonker et al. 2024) at a redshift of $z = 0.4018 \pm 0.0010$ (S. Srivastav et al. 2024; see also J. N. D. van Dalen et al. 2024). (Bottom) A subsection of our MeerKAT discovery image of EP240414a with the source position marked by a pair of black lines. The source has a flux density of 227 ± 13 μJy. We detect clear emission from the possible host galaxy of EP240414a. The MeerKAT restoring beam is shown in the bottom left and is $3\farcs2 \times 3\farcs2$ at a position angle of 0°. A scale bar in the bottom right shows 10 kpc at $z = 0.4$.

AT2024gsa). We obtained a further two observations of EP240414a with MeerKAT, from which source variability can clearly be seen. All of our MeerKAT observations were reduced using the `oxkat` pipeline (I. Heywood 2020), a set of semiautomated scripts for the calibration and imaging of MeerKAT data. `oxkat` performs phase reference calibration using `CASA` (J. P. McMullin et al. 2007; CASA Team et al. 2022), self calibration using `CubiCal` (J. S. Kenyon et al. 2018), and imaging using `WSClean` (A. R. Offringa et al. 2014). Images are cleaned using a Briggs robust weighting of −0.3 (S. D. Briggs 1995), and a circular restoring beam is used to create the clean image. The bright and compact source J1239−1023 was used as the interleaved phase reference calibrator, while PKS B1934−638 was used to set the flux density scale and correct for the bandpass response of the instrument. Typical image rms values are 5–10 μJy beam^{-1}. Our MeerKAT observations are summarized in Table 1.

Table 1
A Summary of Our Radio Observations of EP240414a, Including Measurements from the RACS and VLASS Radio Sky Surveys

Date (dd-mm-yy)	ΔT (days)	Flux Density (μJy)	Frequency (GHz)	Facility
17-10-20	−1275	<905	0.885	ASKAP
20-04-24	6.46	227 ± 13	3	MeerKAT
02-05-24	17.79	<1050	8	ATA
14-05-24	30.48	434 ± 23	3	MeerKAT
15-06-24	62.32	304 ± 17	3	MeerKAT
02-07-24	78.92	320 ± 16	5.5	ATCA
02-07-24	78.92	240 ± 12	9	ATCA
10-07-24	86.72	<420	3	VLASS
23-08-24	130.86	113 ± 12	5.5	ATCA
23-08-24	130.86	73 ± 8	9	ATCA

Note. ΔT is given with respect to MJD 60414.4099.

2.2. Australia Telescope Compact Array

We obtained radio observations of EP240414a with the Australia Telescope Compact Array (ATCA) under program CX576 (PI: Carotenuto). We first observed EP240414a on 2024 July 2 between 06:10 UT and 10:11 UT. ATCA was in its extended 6D configuration. A second observation, under the same program, was performed on 2024 August 23 between 04:40 and 08:30 UT, with the telescope in the more compact 1.5A configuration. For both epochs, data were recorded simultaneously at central frequencies of 5.5 and 9.0 GHz, with 2 GHz of bandwidth at each frequency. We used PKS B1934−638 for bandpass and flux density calibration and J1239–1023 for the complex gain calibration. Data were flagged, calibrated, and imaged using standard procedures within CASA. When imaging, we used a Briggs robust parameter of 0 to balance sensitivity and resolution. Our ATCA observations are summarized in Table 1.

2.3. Allen Telescope Array

As part of a larger survey of EP transients we began observing the field of EP240414a on 2024 May 5 with the Allen Telescope Array (ATA; see W. Farah et al. 2025, in preparation; A. W. Pollak et al. 2025, in preparation). While multiple observing bands were used (see, e.g., J. S. Bright et al. 2022 for details) we report only our most constraining limit at a central frequency of 8 GHz. Observations were reduced with a custom pipeline utilizing CASA for calibration and wsclean for imaging. 3C286 was used to set the absolute flux scale and bandpass response of the instrument, while 1246–075 was used to correct for the time-dependent complex gains. Our ATA observations are summarized in Table 1.

2.4. Archival and Survey Observations

We used the Canadian Initiative for Radio Astronomy Data Analysis Image Cutout Provider[13] to search for observations at the position of EP240414a in large sky area radio surveys. The field of EP240414a was observed with the Karl G. Jansky Very Large Array (VLA) as part of both the VLA Sky Survey (VLASS; M. Lacy et al. 2020) and the NRAO VLA Sky Survey (NVSS; J. J. Condon et al. 1998). Additionally, the Australian Square Kilometer Array Pathfinder Telescope (ASKAP) observed the field as part of the Rapid ASKAP Continuum Survey (RACS; D. McConnell et al. 2020). For the RACS observation there is no source detected at the position of EP240414a on UTC 2020 October 17, with a 3σ upper limit of ∼950 μJy at 885 MHz. In VLASS epoch 3.2 the upper limit is ∼420 μJy at 3 GHz on 2024 July 10 (around 13 weeks after the transient was discovered). The observation as part of NVSS is not constraining compared to the flux density of EP240414a and the limits from RACS and VLASS, and so we do not discuss it further. Radio sky survey observations for EP240414a are summarized in Table 1.

[13] https://cirada.ca/

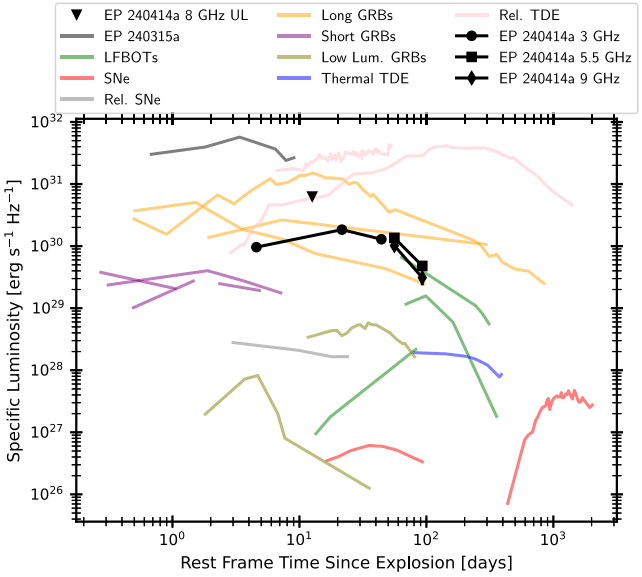

Figure 2. The radio light curve of EP240414a at 3, 5.5, and 9 GHz from MeerKAT and ATCA. The upper limit is from the ATA and is shown with a downward facing arrow. Errors are 1σ and include both a statistical and absolute calibration uncertainty but are smaller than the markers. We show other extragalactic transients to help put our data into context. We include (relativistic) supernova, LFBOTs (D. L. Coppejans et al. 2020), thermal TDEs (K. D. Alexander et al. 2020), relativistic TDEs (T. Eftekhari et al. 2018; L. Rhodes et al. 2023), short GRBs (W. Fong et al. 2021), LGRBs (E. Berger et al. 2003; A. J. van der Horst et al. 2008; J. S. Bright et al. 2019), and low-luminosity GRBs (S. R. Kulkarni et al. 1998; A. M. Soderberg et al. 2006). This figure is based on the one presented in A. Y. Q. Ho et al. (2020). The specific luminosity has been corrected by a factor of (1+z) to account for the cosmological distances of some sources.

3. Results

Our radio observations of EP240414a are fairly sparse, with three observations at 3 GHz with MeerKAT and two ATCA observations both at 5.5 and 9 GHz (see Table 1 and Figure 2). Our 3 GHz light curve shows a clear peak at around ∼30 days postexplosion in the observer reference frame (or ∼20 days in the source rest frame) at 434 ± 21 μJy. While our sampling rate is not high enough to confidently confirm this as the exact peak time at 3 GHz, we can make the approximation that a spectral peak moved through 3 GHz at 30 days postexplosion and therefore take $T_{\rm pk,3\ GHz} = 30$ days and $F_{\rm pk,3\ GHz} = 434 \pm 21$ μJy.

The radio spectral index of our first late time (∼80 days postdetection) ATCA measurement is $\alpha = 0.58 \pm 0.15$, where we use the convention $F_\nu \propto \nu^{-\alpha}$ and fit a simple power law between the two ATCA frequencies. Assuming this is associated with optically thin synchrotron emission, where $\alpha = (p-1)/2$, this implies $p = 2.16 \pm 0.3$, where p is the power-law index of the electron energy distribution

($N(E) \propto E^{-p}$). This indicates that the synchrotron cooling frequency, ν_c, is above 9 GHz at this epoch, as otherwise a spectral slope of $-p/2$ would be expected and imply an extremely hard electron energy distribution. Our second ATCA epoch suggests a marginal steepening of the spectral index to 0.86 ± 0.30, which would imply $p = 2.72 \pm 0.6$, although the values are statistically consistent. In addition to the spectral index we can make crude estimates for the rise and decay indices of the 3 GHz light curves to be $\beta \sim -0.4$ and $\beta \sim 0.5$, respectively, for $F_{3\,\mathrm{GHz}} \propto t^{-\beta}$, although these calculations are obviously sensitive to the exact peak location and assume a constant evolution rate. The late time 3 GHz VLASS measurement indicates that no significant rebrightening occurred at late time.

4. Discussion

4.1. Basic Considerations

We begin with a general discussion of the radio properties of EP240414a in the context of other classes of extragalactic radio transients, particularly (relativistic) supernovae, fast blue optical transients, TDEs (both thermal and relativistic), and gamma-ray bursts both long and short (these comparisons can be appreciated graphically by referring to Figure 2). The observed peak 3 GHz specific luminosity of EP240414a is $\gtrsim 3 \times 10^{30}\,\mathrm{erg\,s^{-1}\,Hz^{-1}}$ and occurs at $T \sim T_0 + 20$ days in the rest frame of the explosion. The timing of this peak is significantly earlier than for the radio counterparts to the luminous fast blue optical transients (LFBOTs), which typically peak closer to 100 days postexplosion in the GHz range and at luminosities closer to $10^{30}\,\mathrm{erg\,s^{-1}\,Hz^{-1}}$ (e.g., A. Y. Q. Ho et al. 2019, 2020; R. Margutti et al. 2019; D. L. Coppejans et al. 2020; J. S. Bright et al. 2022). An exception to this is the LFBOT ZTF19abvkwla, which peaked close to $10^{30}\,\mathrm{erg\,s^{-1}\,Hz^{-1}}$ and at an uncertain peak time before 100 days postdiscovery (A. Y. Q. Ho et al. 2020). This can be seen as the highest luminosity green line in Figure 2 and makes the association between FXTs and LFBOTs hard to rule out.

The peak luminosity of EP240414a also exceeds both regular and relativistic core-collapse supernovae by at least an order of magnitude. In a survey of almost 300 supernovae (including a range of different classifications), M. F. Bietenholz et al. (2021) found a peak specific radio luminosity of $10^{25.5\pm1.6}\,\mathrm{erg\,s^{-1}\,Hz^{-1}}$ (including nondetections), with the brightest source in the entire sample having a peak specific luminosity of $\sim 10^{29}\,\mathrm{erg\,s^{-1}\,Hz^{-1}}$. EP240414a is also more luminous at radio frequencies than all radio-detected superluminous supernovae (SLSNe; T. Eftekhari et al. 2021; R. Margutti et al. 2023), although radio detections of SLSNe are uncommon, especially at early times.

TDEs are also known to produce radio emission, either from a relativistic jet or from nonrelativistic outflow (e.g., S. van Velzen et al. 2016; J. S. Bright et al. 2018; T. Eftekhari et al. 2018; K. D. Alexander et al. 2020; L. Rhodes et al. 2023). These are termed "relativistic" and "thermal" TDEs, respectively. Relativistic TDEs are some of the most luminous radio transients known, with peak specific luminosities exceeding $\sim 10^{32}\,\mathrm{erg\,s^{-1}\,Hz^{-1}}$ and peaking at hundreds of days postexplosion (although the sample of such events is still relatively small). Thermal TDEs peak on similarly long timescales but at much lower specific luminosities of $\sim 10^{29}\,\mathrm{erg\,s^{-1}\,Hz^{-1}}$. These peak luminosities and timescales are incompatible with those seen from EP240414a. Any potential TDE association for EP240414a is further disfavored due to the significant projected offset ($\sim$27 kpc) from the center of the putative host galaxy (P. G. Jonker et al. 2024; A. J. Levan et al. 2024a; S. Srivastav et al. 2024; J. N. D. van Dalen et al. 2024; and see Figure 1).

Finally, we consider EP240414a in the context of GRBs. Long GRB radio afterglows are caused by two major shocks, the forward and reverse, with radiation from each shock peaking between days and hundreds of days postburst, depending on the observing frequency (see, e.g., T. Laskar et al. 2013; A. J. van der Horst et al. 2014; J. S. Bright et al. 2023, for examples from well sampled long GRBs with two clear shock components). The peak radio luminosities of long GRBs span a wide range but are typically between 10^{30} and $\sim 10^{32}\,\mathrm{erg\,s^{-1}\,Hz^{-1}}$ at $\sim$10 days postdiscovery (see, e.g., Figure 6 of P. Chandra & D. A. Frail 2012). The peak luminosity and timescale of EP240414a are both consistent with originating from a long GRB afterglow. The most significant evidence against a GRB progenitor is the location of EP240414a within its host galaxy. Numerous studies (J. S. Bloom et al. 2002; P. K. Blanchard et al. 2016; J. D. Lyman et al. 2017) have shown that long GRBs typically occur close to the center of their host galaxy, with 80% of the sample presented in J. D. Lyman et al. (2017) located within $\sim$3 kpc. In the sample presented in P. K. Blanchard et al. (2016) there were no offsets above 20 kpc in their sample of $\sim$100 LGRBs. In fact, the galactic offset of EP240414a ($\sim$27 kpc) is much more consistent with those seen for short gamma-ray bursts, with W.-F. Fong et al. (2022) finding that a significant fraction of their sample fell outside of a 10 kpc radius and the most distant above 50 kpc in separation. However, EP240414a has been associated with a Type Ic broad line supernova (A. J. Levan et al. 2024a; J. N. D. van Dalen et al. 2024), a supernova class solidly associated with LGRBs (see J. Hjorth & J. S. Bloom 2012 for a review). The offset discrepancy was also commented on by J. N. D. van Dalen et al. (2024), who noted that LFBOTs can have host offsets comparable to EP240414a and that there is only weak star formation at the location of EP240414a in its host galaxy. While luminosity rise-time arguments are not conclusive in determining the progenitor of a source, based on the arguments above we suggest that EP240414a is likely an LGRB that occurred in an unusual location in its host galaxy. The lack of reported gamma-ray emission suggests that this GRB could have had a low isotropic gamma-ray luminosity, or the radio emission could have been seen from off-axis. For example, the lack of detection by Konus-Wind suggests that the isotropic equivalent gamma-ray energy was below $\sim 10^{51}$ erg, based on the sample presented in A. Tsvetkova et al. (2017; their Figure 8). This energy is at the low end of the distribution for long GRBs, but not unusually so (see Figure 1 in D. A. Perley et al. 2014). Following up sources detected with the EP could help elucidate the distinction, or lack thereof (E. Nakar 2015), between low-luminosity LGRBs and regular LGRBs, potentially driven by differences in circumburst material or viewing angle (E. Liang et al. 2007; O. S. Salafia et al. 2016).

4.2. Comparison with FXT EP240315a

The first FXT with a radio counterpart, EP240315a, was associated with a high-redshift ($z = 4.9$) gamma-ray burst (J. H. Gillanders et al. 2024; A. J. Levan et al. 2024b; Y. Liu et al. 2025). The specific radio luminosity of EP240315a (also

at 3 GHz) was around 1 order of magnitude larger than the (observed) peak for EP240414a and occurred 1 order of magnitude earlier (although at 5.5 GHz, not 3 GHz). While the light-curve properties of EP240315a and EP240414a are not similar, both sources are consistent with the diversity in radio light curves seen from long GRBs (see, e.g., P. Chandra & D. A. Frail 2012).

4.3. Minimum Energy Constraints

4.3.1. Low Bulk Velocity

We start by considering our radio observations of EP240414a in the context of minimum energy arguments under the assumption that the emitting region is not moving relativistically. It can be shown (e.g., M. A. Scott & A. C. S. Readhead 1977) that the total energy of a synchrotron emitting region, which is the combined energy of the magnetic field and electrons, has a strong minimum as a function of magnetic field strength. This minimum is known as the equipartition energy as it occurs close to (but not exactly at) the magnetic field strength where the energy in the magnetic field and electrons is equal. If the size of the emitting region is known then the magnetic field and therefore the minimum energy can be calculated.

For the majority of extragalactic transients the size of the emitting region is unknown and so an additional constraint relating the magnetic field and the size of the emitting region is required. Such a condition exists if the emitting region is seen to be self-absorbed to synchrotron radiation at a given frequency, which allows for the minimum energy, magnetic field, and size (and therefore velocity) to be uniquely constrained. Focusing on the energy and size, following T. Matsumoto & T. Piran (2023), we have

$$E_{\rm eq,N} = 6.2 \times 10^{49} d_{L,28}^{40/17} F_{\nu,\rm mJy}^{20/17} \nu_{10}^{-1} (1+z)^{-37/17} \ {\rm erg} \quad (1a)$$

$$R_{\rm eq,N} = 1.9 \times 10^{17} d_{L,28}^{16/17} F_{\nu,\rm mJy}^{8/17} \nu_{10}^{-1} (1+z)^{-25/17} \ {\rm cm} \quad (1b)$$

for a completely filled emitting region in the Newtonian limit. The distance to the source ($d_{L,28}$) is given in units of 10^{28} cm, the flux density ($F_{\nu,\rm mJy}$) is given in mJy, the frequency (ν) is given in units of 10 GHz, and z is the redshift of the source. Using the peak of our 3 GHz light curve this implies $E_{\rm eq} = 1.5 \times 10^{49}$ erg and $R_{\rm eq} = 1.8 \times 10^{17}$ cm. At 20 days postexplosion (in the source rest frame) this size implies an expansion velocity $\beta_{\rm eq,N} \approx 3.3c$. Note that while T. Matsumoto & T. Piran (2023) assumes a different geometry to R. Fender & J. Bright (2019; a conical outflow and an expanding sphere, respectively), the derived radii and energies agree to within a factor of order unity. This result implies that the source has a significant, likely at least mildly relativistic, expansion velocity.

4.3.2. Relativistic Considerations

In the relativistic regime, minimum energy arguments become more complex due to the dependence of parameters on the bulk Lorentz factor (Γ) and the angle to the line of sight (θ) to the observer. This manifests through the relativistic Doppler factor $\delta = \Gamma^{-1}(1 - \beta \cos\theta)^{-1}$ (as well as through the filling factors, which have a dependence on Γ). The addition of these parameters means that no global minimum exists for the energy as a function of radius, Γ, and θ, and instead the total energy must be left as

$$e(R, \theta, \Gamma) = E/E_{\rm eq,N} = \frac{\Gamma}{\delta_{\rm D}^{\frac{43}{17}}} \left[\frac{11}{17} \left(\frac{r}{\Gamma \delta_{\rm D}^{-\frac{7}{17}}} \right)^{-6} + \frac{6}{17} \left(\frac{r}{\Gamma \delta_{D}^{-\frac{7}{17}}} \right)^{11} \right] \quad (2)$$

following T. Matsumoto & T. Piran (2023), where $r = R/R_{\rm eq,N}$. This reduces to the Newtonian case for Γ, $\delta_{\rm D} \to 1$. When fixing one of the parameters (R, θ, or Γ), a family of relativistic minimum energy solutions exists for the pair of remaining parameters. To make progress, we must include an additional relationship between $r = R/R_{\rm eq,N}$, Γ, and θ, which in both R. Barniol Duran et al. (2013) and T. Matsumoto & T. Piran (2023) is $r = (\beta/\beta_{\rm eq,N})\Gamma\delta_{\rm D}$, where

$$\beta_{\rm eq,N} = \frac{(1+z)R_{\rm eq,N}}{ct} \approx 0.73 \left[\frac{F_{p,\rm mJy}^{\frac{8}{17}} d_{L,28}^{\frac{16}{17}} \eta^{\frac{35}{51}}}{\nu_{p,10} (1+z)^{\frac{8}{17}}} \left(\frac{t}{100 \ {\rm days}} \right)^{-1} \right] f_A^{-\frac{7}{17}} f_V^{-\frac{1}{17}} \quad (3)$$

is the Newtonian expansion velocity, which can be calculated directly from the peak in the radio spectrum, as was done in the previous section (see also R. Barniol Duran et al. 2013; R. Fender & J. Bright 2019). The value of η depends on the ordering of $\nu_{\rm m}$ and $\nu_{\rm sa}$ (the frequencies corresponding to emission from the minimum electron energy in the distribution, and the self absorption frequency, respectively) and is equal to 1 if $\nu_{\rm sa} > \nu_{\rm m}$ (i.e., the spectral peak is due to self absorption) and equal to $\nu_{\rm m}/\nu_{\rm sa}$ if $\nu_{\rm sa} < \nu_m$ (i.e., the spectral peak is due to the minimum electron energy). Area and volume filling factors are given by f_A and f_V, respectively. Recasting Equation (3) into units more appropriate for Galactic transients reproduces Equation (28) from R. Fender & J. Bright (2019) with differences of order unity due to the different assumed geometries.

Assuming that the peak we measure in the MeerKAT light curve is due to synchrotron self absorption ($\eta = 1$) and taking $f_A = f_V = 1$, we derive $\beta_{\rm eq,N} \approx 3.3$ (as before). Recasting Equation (2) in terms of just Γ and θ it can be seen that there is a family of minimum energy solutions for (Γ, θ) for a given $\beta_{\rm eq,N}$, where both on- and off-axis jet solutions exist for different jet angles, depending on the Lorentz factor as $\theta = 1/\Gamma$. We note that the condition $\beta_{\rm eq,N} \approx 3.3$ is robust to the exact values of η, f_A, and f_V as $\eta \geqslant 1$ and $f_A, f_V \leqslant 1$. We show the minimum energy parameter space for $\beta_{\rm eq,N} = 3.3$ in Figure 3. Considering only on-axis solutions, Figure 3 demonstrates that a modest bulk Lorentz $\Gamma \gtrsim 1.6$ satisfies the relativistic minimum energy condition for $\theta \lesssim 0.4 \approx 20^\circ$. Formally, T. Matsumoto & T. Piran (2023) identify an approximation for the minimum on-axis Lorentz factor in the case that $\theta \ll 1$ and $\Gamma \gg 1$ as $\Gamma_{\rm on} \approx \beta_{\rm eq,N}^{17/24}/2$, which is not appropriate for EP240414a as it significantly underpredicts the on-axis Lorentz factor to be $\Gamma_{\rm on} \approx 1.2$ (see Figure 3). A more general solution for the jet speed corresponding to the

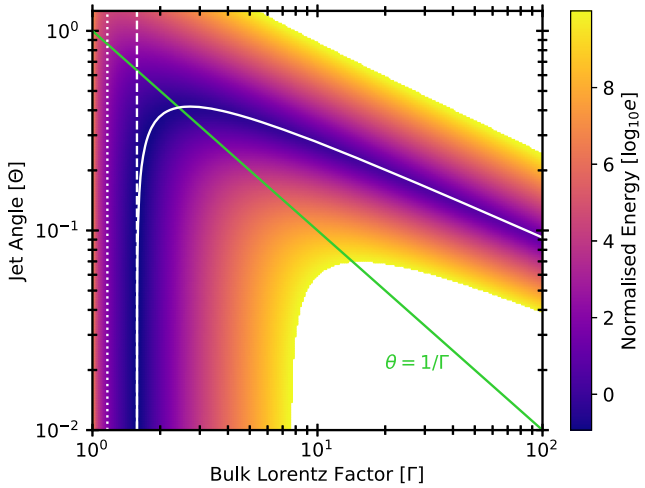

Figure 3. The relativistic energy as a function of bulk Lorentz factor and jet angle for $\beta_{\rm eq,N} = 3.3$, as is appropriate for EP240414a. The green line divides on- and off-axis solutions to the left and right, respectively. We only show solutions below 10^{10} times the minimum energy in the Newtonian limit. The solid white line marks the minimum energy for a given angle and Lorentz factor. The dashed white line shows the asymptotic limit of Γ, which satisfies the minimum energy condition for $\theta \rightarrow 1$ according to Equation (4). The dotted white line shows the solution from T. Matsumoto & T. Piran (2023), which breaks down for moderate values of $\beta_{\rm eq,N}$.

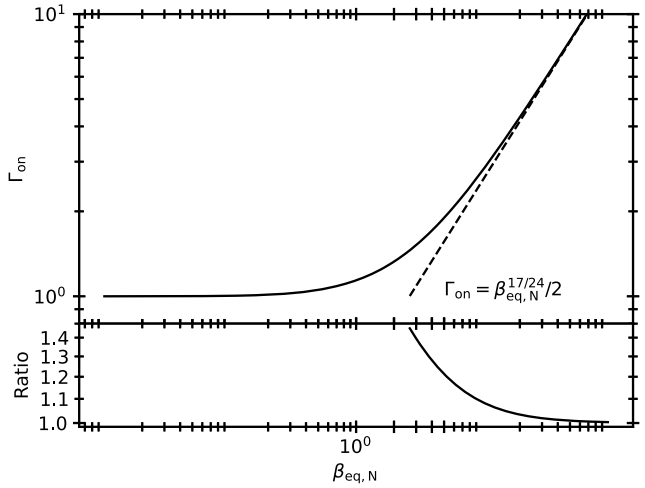

Figure 4. Solution for the minimum bulk Lorentz factor for Equation (4) and the one given in T. Matsumoto & T. Piran (2023), which becomes significantly incorrect for $\beta_{\rm eq,N} \lesssim 15$, at which point the ratio becomes larger than 1.05. At $\beta_{\rm eq,N} \lesssim 9$ the ratio surpasses 1.1.

relativistic minimum energy in the on-axis case exists as

$$\beta_{\rm eq,N}^{\frac{17}{12}} = \beta_{\rm on}^{\frac{17}{12}} \left[\frac{1+\beta_{\rm on}}{1-\beta_{\rm on}} \right], \tag{4}$$

which can be solved for $\beta_{\rm on}$, and therefore $\Gamma_{\rm on}$, numerically. We demonstrate the solution to Equation (4) in Figure 3 for $\beta_{\rm eq,N} = 3.3$. Recasting Equation (4) in terms of $\Gamma_{\rm on}$ and taking $\Gamma \gg 1$ reproduces the result given in T. Matsumoto & T. Piran (2023; their Equation (34)). We show $\Gamma_{\rm on}$ calculated via these two different methods in Figure 4 and demonstrate that the approximation in T. Matsumoto & T. Piran (2023) is inappropriate for $\beta_{\rm eq,N} \lesssim 9$ ($\beta_{\rm eq,N} \lesssim 15$) at the 10% (5%) level.

For our measured $\beta_{\rm eq,N} = 3.3$ we have that $\beta_{\rm on} \approx 0.8$ or $\Gamma_{\rm on} \approx 1.6$. We can compare this with simply considering the

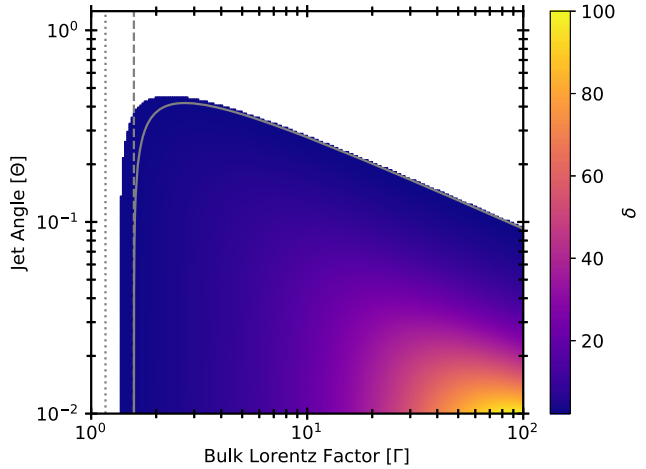

Figure 5. The Doppler factor as a function of Γ and θ. The region of the plot colored white violates the condition $\delta_D^{49/34} > 3.3$, and therefore the boundary is defined as $\delta_D^{49/34} = 3.3$. It can be seen that the minimum energy locus is approximated by the boundary, and they converge as $\beta \rightarrow 1$ (see Figure 29 in T. Matsumoto & T. Piran 2023, and R. Fender & J. Bright 2019). The gray lines are the same as the white ones in Figure 3.

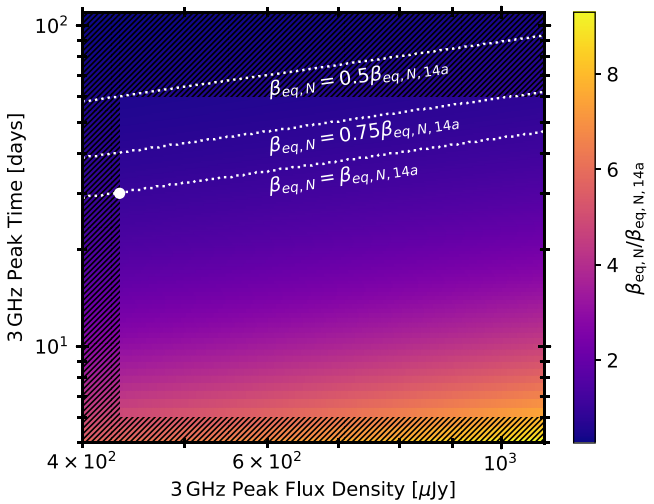

Figure 6. Measured $\beta_{\rm eq,N}$ as a function of an uncertain peak flux density and time expressed as a ratio to $\beta_{\rm eq,N}$ assuming a peak at ∼30 days postdiscovery (giving $\beta_{\rm eq,N,14a} \approx 3.3$), which is marked on the plot by a white circle. Hatched areas mark regions ruled out by our observations. We show three white dotted lines to demonstrate $\beta_{\rm eq,N} = (0.5, 0.75, 1) \times \beta_{\rm eq,N,14a}$. A majority of the allowed parameter space would imply $\beta_{\rm eq,N}$ higher than the one we measure from our assumed peak, and no solutions exist for $\beta_{\rm eq} \lesssim 1.7$.

Doppler factor required for an apparent velocity of $3.3c$ to appear subrelativistic. From R. Fender & J. Bright (2019) this requires $\delta_D^{49/34} \gtrsim 3.3$, implying a velocity above $0.7c$ and a jet angle below ≃25°. This is similar to the result derived using the methodology outlined above. Further, the condition $\delta_D^{49/34} = \beta_{\rm eq,N}$ provides a reasonable approximation to the minimum energy as a function of Γ and θ (the solid white line in Figure 3) and approaches it in the limit $\beta \rightarrow 1$. We demonstrate this in Figure 5 for $\beta_{\rm eq,N} = 3.3$.

Our results imply that the emitting region responsible for the radio emission from EP240414a was expanding at least moderately relativistically at 30 days postexplosion. The Newtonian equipartition energy ($E_{\rm eq,N} \approx 1.5 \times 10^{49}$ erg) is reduced by a factor of ∼10 for the on-axis relativistic case (e.g., $e_{\rm on} = 0.1$). The potentially large Lorentz factors and uncertain

geometries of GRB jets make comparison challenging, for example if the opening angle of the jet $\theta_j > 1/\Gamma$ then the energy is underestimated by a factor of $4\Gamma^2(1 - \cos\theta_j)$.

Due to our sparse temporal sampling there is significant uncertainty on the peak flux density and frequency at 3 GHz. We demonstrate in Figure 6 that only a small region of the peak flux density and peak time parameter space would have produced a $\beta_{\rm eq,N}$ less than the one we inferred, and no solutions exist for $\beta_{\rm eq,N} \lesssim 2$ (or $\Gamma_{\rm on} \gtrsim 1.3$). While the upper bound of the peak flux density is not constrained, our ATA observations indicate that EP240414a was likely not more than a few mJy at peak.

5. Conclusions

We present radio observations of EP240414a, the second FXT with a radio counterpart. The rise time and peak luminosity of EP240414a distinguish it from regular supernovae and TDEs but are commonly seen from gamma-ray bursts and perhaps from the most luminous fast blue optical transients. Due to the association of EP240414a with a Ic broad line supernova (J. N. D. van Dalen et al. 2024), a short gamma-ray burst is disfavored despite the large spatial offset from the host galaxy. Based on minimum energy arguments and the presence of a turnover in our 3 GHz light curve of EP2402414a, we place approximate limits on the bulk Lorentz factor of the outflow of $\Gamma \gtrsim 1.6$ with an energy $\sim 10^{48}$ erg in the on-axis case. Additionally, we extend the results presented in T. Matsumoto & T. Piran (2023) to show that a general minimum energy solution for on-axis ($\theta \to 0$) sources exists for any measured apparent source velocity, without the assumption of a large bulk Lorentz factor (Equation (4)). Our observations suggest that at least a moderately relativistic outflow was present in EP240414a and that the progenitor and engine was likely a collapsar, such as those that produce the known population of gamma-ray bursts. The absence of a reported gamma-ray counterpart to EP240414a suggests that it could be a GRB with a relatively low isotropic equivalent gamma-ray energy (below $\sim 10^{51}$ erg), or that the radio emission is driven by a mildly off-axis jet (as has been suggested by, e.g., D. Ibrahimzade et al. 2025; H. C. I. Wichern et al. 2024) or a cocoon associated with a choked jet (e.g., O. Bromberg et al. 2012). Such scenarios have been suggested for relativistic supernovae such as SN 2009bb (e.g., A. M. Soderberg et al. 2010); however, EP240414a is significantly more luminous than such events. Based on the observations presented in this work, J. H. Gillanders et al. (2024), and R. Ricci et al. (2025), we suggest that a significant fraction of EP FXTs are associated with the collapse of massive stars and their afterglows.

In the approximately half a year that the EP has been operating it has already redefined the study of the transient X-ray sky, allowing for prompt multiwavelength follow-up of FXTs. During this time, EP FXTs have been firmly associated with flaring stars and cataclysmic variables, and, in the cases of EP240315a and EP240414a, the detected radio emission indicates the production of at least moderately relativistic outflows. Over the coming years the number of FXTs with multiwavelength counterparts is due to increase dramatically, and only through further dedicated observing campaigns will the range of FXT progenitors be elucidated.

Acknowledgments

The MeerKAT telescope is operated by the South African Radio Astronomy Observatory, which is a facility of the National Research Foundation, an agency of the Department of Science and Innovation.

This work has made use of the "MPIfR *S*-band receiver system" designed, constructed and maintained by funding of the MPI für Radioastronomy and the Max-Planck-Society.

The Australia Telescope Compact Array is part of the Australia Telescope National Facility (https://ror.org/05qajvd42), which is funded by the Australian Government for operation as a National Facility managed by CSIRO. We acknowledge the Gomeroi people as the Traditional Owners of the Observatory site.

The Allen Telescope Array (ATA) refurbishment program and its ongoing operations are being substantially funded through the Franklin Antonio Bequest. Additional contributions from Frank Levinson, Greg Papadopoulos, the Breakthrough Listen Initiative, and other private donors have been instrumental in the renewal of the ATA. Breakthrough Listen is managed by the Breakthrough Initiatives, sponsored by the Breakthrough Prize Foundation. The Paul G. Allen Family Foundation provided major support for the design and construction of the ATA, alongside contributions from Nathan Myhrvold, Xilinx Corporation, Sun Microsystems, and other private donors. The ATA has also been supported by contributions from the US Naval Observatory and the US National Science Foundation.

The National Radio Astronomy Observatory is a facility of the National Science Foundation operated under cooperative agreement by Associated Universities, Inc.

This scientific work uses data obtained from Inyarrimanha Ilgari Bundara/the Murchison Radio-astronomy Observatory. We acknowledge the Wajarri Yamaji People as the Traditional Owners and native title holders of the Observatory site. CSIRO's ASKAP radio telescope is part of the Australia Telescope National Facility (https://ror.org/05qajvd42). Operation of ASKAP is funded by the Australian Government with support from the National Collaborative Research Infrastructure Strategy. ASKAP uses the resources of the Pawsey Supercomputing Research Centre. Establishment of ASKAP, Inyarrimanha Ilgari Bundara, the CSIRO Murchison Radio-astronomy Observatory, and the Pawsey Supercomputing Research Centre are initiatives of the Australian Government, with support from the Government of Western Australia and the Science and Industry Endowment Fund. This paper includes archived data obtained through the CSIRO ASKAP Science Data Archive, CASDA (https://data.csiro.au).

J.M. acknowledges funding from a Royal Society University Research Fellowship. A.M. acknowledges support from a Leverhulme Trust International Professorship grant (number LIP-202-014). We thank Anna Ho for making the code associated with A. Y. Q. Ho et al. (2020) publicly available. F.C. acknowledges support from the Royal Society through the Newton International Fellowship program (NIF/R1/211296). S.J.S. acknowledges funding from STFC grants ST/Y001605/1, ST/X006506/1, and ST/T000198/1, a Royal Society Research Professorship, and the Hintze Charitable Foundation.

Facilities: ASKAP, ATA, ATCA, MeerKAT, VLA.

Software: astropy (Astropy Collaboration et al. 2013), CASA (J. P. McMullin et al. 2007; CASA Team et al. 2022), CubiCal (J. S. Kenyon et al. 2018), WSClean (A. R. Offringa et al. 2014).

ORCID iDs

Joe S. Bright https://orcid.org/0000-0002-7735-5796
Francesco Carotenuto https://orcid.org/0000-0002-0426-3276
Carmen Choza https://orcid.org/0009-0008-0662-1293
Peter G. Jonker https://orcid.org/0000-0001-5679-0695
Stephen J. Smartt https://orcid.org/0000-0002-8229-1731
David R. DeBoer https://orcid.org/0000-0003-3197-2294
Wael Farah https://orcid.org/0000-0002-0161-7243
James Matthews https://orcid.org/0000-0002-3493-7737
Alexander W. Pollak https://orcid.org/0000-0002-3430-7671
Lauren Rhodes https://orcid.org/0000-0003-2705-4941
Andrew Siemion https://orcid.org/0000-0003-2828-7720

References

Alexander, K. D., van Velzen, S., Horesh, A., & Zauderer, B. A. 2020, SSRv, 216, 81
Alp, D., & Larsson, J. 2020, ApJ, 896, 39
Aryan, A., Yang, S., Chen, T. W., et al. 2024, GCN, 36094, 1
Astropy Collaboration, Robitaille, T. P., Tollerud, E. J., et al. 2013, A&A, 558, A33
Barniol Duran, R., Nakar, E., & Piran, T. 2013, ApJ, 772, 78
Bauer, F. E., Treister, E., Schawinski, K., et al. 2017, MNRAS, 467, 4841
Berger, E., Kulkarni, S. R., Pooley, G., et al. 2003, Natur, 426, 154
Bietenholz, M. F., Bartel, N., Argo, M., et al. 2021, ApJ, 908, 75
Blanchard, P. K., Berger, E., & Fong, W.-f. 2016, ApJ, 817, 144
Bloom, J. S., Kulkarni, S. R., & Djorgovski, S. G. 2002, AJ, 123, 1111
Briggs, D. S. 1995, PhD thesis, New Mexico Institute of Mining and Technology
Bright, J., Carotenuto, F., Jonker, P. G., Fender, R., & Smartt, S. 2024, GCN, 36362, 1
Bright, J. S., Fender, R. P., Motta, S. E., et al. 2018, MNRAS, 475, 4011
Bright, J. S., Horesh, A., van der Horst, A. J., et al. 2019, MNRAS, 486, 2721
Bright, J. S., Margutti, R., Matthews, D., et al. 2022, ApJ, 926, 112
Bright, J. S., Rhodes, L., Farah, W., et al. 2023, NatAs, 7, 986
Bromberg, O., Nakar, E., Piran, T., & Sari, R. 2012, ApJ, 749, 110
Buckley, D. A. H., Monageng, I., Aydi, E., Scaringi, S., & Charles, P. A. 2024, ATel, 16554, 1
Carotenuto, F., Bright, J., Jonker, P. G., Fender, R., & Rhodes, L. 2024, GCN, 35961, 1
CASA Team, Bean, B., Bhatnagar, S., et al. 2022, PASP, 134, 114501
Chandra, P., & Frail, D. A. 2012, ApJ, 746, 156
Condon, J. J., Cotton, W. D., Greisen, E. W., et al. 1998, AJ, 115, 1693
Coppejans, D. L., Margutti, R., Terreran, G., et al. 2020, ApJL, 895, L23
Eappachen, D., Jonker, P. G., Fraser, M., et al. 2022, MNRAS, 514, 302
Eappachen, D., Jonker, P. G., Levan, A. J., et al. 2023, ApJ, 948, 91
Eappachen, D., Jonker, P. G., Quirola-Vásquez, J., et al. 2024, MNRAS, 527, 11823
Eftekhari, T., Berger, E., Zauderer, B. A., Margutti, R., & Alexander, K. D. 2018, ApJ, 854, 86
Eftekhari, T., Margalit, B., Omand, C. M. B., et al. 2021, ApJ, 912, 21
Fender, R., & Bright, J. 2019, MNRAS, 489, 4836
Fletcher, C., Lesage, S., Jenke, P. & Fermi-GBM Team 2024, GCN, 35776, 1
Fong, W., Laskar, T., Rastinejad, J., et al. 2021, ApJ, 906, 127
Fong, W.-F., Nugent, A. E., Dong, Y., et al. 2022, ApJ, 940, 56
Gehrels, N., Ramirez-Ruiz, E., & Fox, D. B. 2009, ARA&A, 47, 567
Gillanders, J. H., Rhodes, L., Srivastav, S., et al. 2024, ApJL, 969, L14
Glennie, A., Jonker, P. G., Fender, R. P., Nagayama, T., & Pretorius, M. L. 2015, MNRAS, 450, 3765
Guan, J., Li, C. K., Chen, Y., et al. 2024, GCN, 36129, 1
Heywood, I., 2020 oxkat: semi-automated imaging of MeerKAT observations, Astrophysics Source Code Library, ascl:2009.003
Hjorth, J., & Bloom, J. S. 2012, in Gamma-Ray Bursts, ed. C. Kouveliotou, R. A. M. J. Wijers, & S. Woosley (Cambridge: Cambridge Univ. Press), 169
Ho, A. Y. Q., Perley, D. A., Kulkarni, S. R., et al. 2020, ApJ, 895, 49
Ho, A. Y. Q., Phinney, E. S., Ravi, V., et al. 2019, ApJ, 871, 73
Ibrahimzade, D., Margutti, R., Bright, J. S., et al. 2025, ApJ, 980, 92
Jonker, P. G., Glennie, A., Heida, M., et al. 2013, ApJ, 779, 14
Jonker, P. G., Levan, A. J., Malesani, D. B., et al. 2024, GCN, 36110, 1
Kenyon, J. S., Smirnov, O. M., Grobler, T. L., & Perkins, S. J. 2018, MNRAS, 478, 2399
Kulkarni, S. R., Frail, D. A., Wieringa, M. H., et al. 1998, Natur, 395, 663
Lacy, M., Baum, S. A., Chandler, C. J., et al. 2020, PASP, 132, 035001
Laskar, T., Berger, E., Zauderer, B. A., et al. 2013, ApJ, 776, 119
Levan, A. J., Jonker, P. G., Saccardi, A., et al. 2024b, arXiv:2404.16350
Levan, A. J., van Dalen, J., Jonker, P., et al. 2024a, GCN, 36355, 1
Lian, T. Y., Pan, X., Ling, Z. X., et al. 2024, GCN, 36091, 1
Liang, E., Zhang, B., Virgili, F., & Dai, Z. G. 2007, ApJ, 662, 1111
Liu, M. J., Li, D. Y., Liu, Y., et al. 2024, ATel, 16514, 1
Liu, Y., Sun, H., Xu, D., et al. 2025, NatAs, in press (arXiv:2404.16425)
Lyman, J. D., Levan, A. J., Tanvir, N. R., et al. 2017, MNRAS, 467, 1795
Margutti, R., Bright, J. S., Matthews, D. J., et al. 2023, ApJL, 954, L45
Margutti, R., Metzger, B. D., Chornock, R., et al. 2019, ApJ, 872, 18
Matsumoto, T., & Piran, T. 2023, MNRAS, 522, 4565
McConnell, D., Hale, C. L., Lenc, E., et al. 2020, PASA, 37, e048
McMullin, J. P., Waters, B., Schiebel, D., Young, W., & Golap, K. 2007, in ASP Conf. Ser. 376, Astronomical Data Analysis Software and Systems XVI, ed. R. A. Shaw, F. Hill, & D. J. Bell (San Francisco, CA: ASP), 127
Nakar, E. 2015, ApJ, 807, 172
Novara, G., Esposito, P., Tiengo, A., et al. 2020, ApJ, 898, 37
Offringa, A. R., McKinley, B., Hurley-Walker, N., et al. 2014, MNRAS, 444, 606
Perley, D. A., Cenko, S. B., Corsi, A., et al. 2014, ApJ, 781, 37
Quirola-Vásquez, J., Bauer, F. E., Jonker, P. G., et al. 2022, A&A, 663, A168
Quirola-Vásquez, J., Bauer, F. E., Jonker, P. G., et al. 2023, A&A, 675, A44
Rhodes, L., Bright, J. S., Fender, R., et al. 2023, MNRAS, 521, 389
Ricci, R., Troja, E., Yang, Y., et al. 2025, ApJL, 979, L28
Salafia, O. S., Ghisellini, G., Pescalli, A., Ghirlanda, G., & Nappo, F. 2016, MNRAS, 461, 3607
Scott, M. A., & Readhead, A. C. S. 1977, MNRAS, 180, 539
Soderberg, A. M., Berger, E., Page, K. L., et al. 2008, Natur, 453, 469
Soderberg, A. M., Chakraborti, S., Pignata, G., et al. 2010, Natur, 463, 513
Soderberg, A. M., Kulkarni, S. R., Nakar, E., et al. 2006, Natur, 442, 1014
Srivastav, S., Chen, T. W., Gillanders, J. H., et al. 2024, ApJL, 978, L21
Tsvetkova, A., Frederiks, D., Golenetskii, S., et al. 2017, ApJ, 850, 161
van Dalen, J. N. D., Levan, A. J., Jonker, P. G., et al. 2024, arXiv:2409.19056
van der Horst, A. J., Kamble, A., Resmi, L., et al. 2008, A&A, 480, 35
van der Horst, A. J., Paragi, Z., de Bruyn, A. G., et al. 2014, MNRAS, 444, 3151
van Velzen, S., Anderson, G. E., Stone, N. C., et al. 2016, Sci, 351, 62
Wichern, H. C. I., Ravasio, M. E., Jonker, P. G., et al. 2024, A&A, 690, A101
Xue, Y. Q., Zheng, X. C., Li, Y., et al. 2019, Natur, 568, 198
Yuan, W., Zhang, C., Chen, Y., & Ling, Z. 2022, in Handbook of X-ray and Gamma-ray Astrophysics, ed. C. Bambi & A. Sangangelo (Berlin: Springer), 86